

Unfolding the Hong-Ou-Mandel interference between heralded photons from narrowband twin beams

K. Laiho^{a,*}, T. Dirmeier^{b,c}, G. Shafiee^{b,c}, and Ch. Marquardt^{c,b}

^a*German Aerospace Center (DLR e.V.), Institute of Quantum Technologies, Wilhelm-Runge-Str. 10, 89081 Ulm, Germany*

^b*Max Planck Institute for the Science of Light, Staudtstr. 2, 91058 Erlangen, Germany*

^c*Friedrich-Alexander-Universität Erlangen-Nürnberg (FAU), Department of Physics, Staudtstr. 7/B2, 91058 Erlangen, Germany*

Abstract

The Hong-Ou-Mandel (HOM) interference is one of the most intriguing quantum optical phenomena and crucial in performing quantum optical communication and computation tasks. Lately, twin beam emitters such as those relying on the process of parametric down-conversion (PDC) have become confident sources of heralded single photons. However, if the pump power is high enough, the pairs produced via PDC—often called signal and idler—incorporate multiphoton contributions that usually distort the investigated quantum features. Here, we derive the temporal characteristics of the HOM interference between heralded states from two independent narrowband PDC sources. Apart from the PDC multiphoton content, our treatment also takes into account effects arriving from an unbalanced beam splitter ratio and optical losses. We perform a simulation in the telecommunication wavelength range and provide a useful tool for finding the optimal choice for PDC process parameters. Our results offer insight in the properties of narrowband PDC sources and turn useful when driving quantum optical applications with them.

Keywords: Hong-Ou-Mandel interference, two-mode squeezed vacuum, twin beams, multiphoton processes, parametric down-conversion

1. Introduction

The two-photon quantum interference named after the seminal experiment of Hong, Ou and Mandel provides evidence of photon bunching and stems from the true quantum features of light [1]. Today, this quantum phenomenon is one of the most important building blocks of photonic quantum information and communication applications [2]. Many applications require spectrally tailored single-photon sources in order to guarantee the applicability of the quantum light with the so-called quantum hardware [3, 4, 5].

Regarding photon-pair generation processes, the HOM interference between independent heralded single photons has vastly been investigated on platforms relying both on the four-wave mixing [6, 7, 8, 9] and parametric down-conversion (PDC) [10, 11, 12, 13]. Recently, highly versatile and conveniently tunable sources of photon pairs—usually denoted as signal and idler—have successfully been demonstrated with different spectro-temporal characteristic [14, 15, 16, 17]. When utilizing photon-pair processes in the HOM interference experiments, care has to be taken since their multiphoton contributions are known to diminish the visibility of the two-photon interference dip. Such results have been reported at least when investigating the indistinguishability of signal and idler [18, 19, 20] and when examining the HOM interference between heralded states from different photon-pair sources [7, 21], as well as between heralded single photons and coherent states [22]. In case the multiphoton contributions are not taken into account the interpretation of the quantum features of the manipulated light can be falsified. In other cases, recently spectral multiplexing have been proposed and realized to counteract the drawback of PDC multiphoton contributions [23].

*Corresponding author

Email address: kaisa.laiho@dlr.de (K. Laiho)

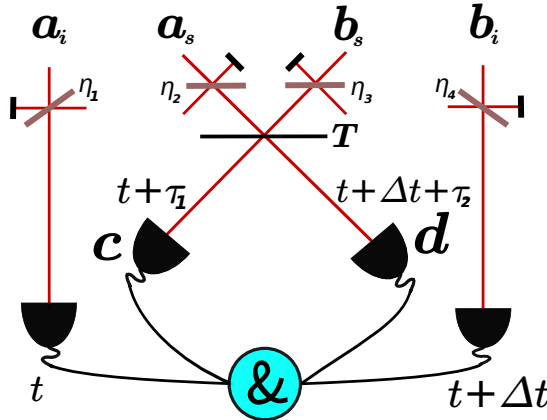


Figure 1: Sketch of the HOM interference experiment with two heralded photons from different PDC sources. The idler (i) beams of the two narrowband PDC processes, which we label here with a and b , are used as the heralds, while the signal (s) beams are sent to the input ports of the beam splitter having the transmittance T . Each beam path a_i , a_s , b_i and b_s is objected to the optical loss, modeled as a beam splitter with the transmittance corresponding to the efficiency, at which the mode is detected. Vacuum modes are not explicitly denoted. For further details see text.

The spectral and temporal characteristics of photons emitted via PDC are related to each other with the Fourier transform. Often, the spectral properties of these sources can be easily accessed [24] and measured at the few photon level with high-resolution spectrographs [25]. Contrariwise, the coincidence discrimination mostly happens in the temporal domain. We take use of the spectral PDC properties to derive the temporal characteristics of the HOM interference dip between heralded states from two independent narrowband PDC sources. Our treatment takes into account the PDC multiphoton contributions and other experimental imperfections such as optical losses and an unbalanced beam splitter ratio. Instead of operating in the photon-number basis our derivation is based on evaluating the required expectation values directly with PDC states, in other words, two-mode squeezed vacuum states, which allows to easily capture the full state characteristics [26, 27]. We simulate the four-fold coincidence probability in the telecommunication wavelength range assuming Gaussian PDC spectra and indicate how the visibility of the HOM interference dip degrades in terms of the PDC multiphoton contributions. We note that each platform producing continuous-wave photon pairs has its highly individual spectral characteristics that needs to be thoroughly scrutinized to gain an accurate estimate of the background effects [28, 29]. Further, we investigate the integral over the temporal characteristics of signal and idler cross-correlation to show the practicality of this figure-of-merit as a PDC process parameter [30]. We believe our results can enhance the efficient utilization of narrowband PDC sources in quantum optical applications and help reaching a high visibility in the HOM interference experiment.

2. Derivation of the temporal characteristics of the HOM interference

We investigate the HOM interference between heralded photons from two independent narrowband PDC sources taking into account the PDC multiphoton contributions, optical losses at the paths of signal and idler beams as well as an unbalanced beam splitter ratio. The optical arrangement is sketched in Fig. 1 and the depicted four-fold coincidence probability can be derived via [7]

$$P(t, t + \tau_1, t + \Delta t + \tau_2, t + \Delta t) = \eta_1 \eta_2 \langle \hat{a}_i^\dagger(t) \hat{b}_i^\dagger(t + \Delta t) \hat{c}^\dagger(t + \tau_1) \hat{d}^\dagger(t + \Delta t + \tau_2) \hat{d}(t + \Delta t + \tau_2) \hat{c}(t + \tau_1) \hat{b}_i(t + \Delta t) \hat{a}_i(t) \rangle, \quad (1)$$

in which \hat{a}_μ^\dagger [\hat{a}_μ] and \hat{b}_μ^\dagger [\hat{b}_μ] ($\mu = s, i$) stand for the photon creation [annihilation] in the signal (s) and idler (i) modes of the two investigated PDC processes, η_ξ ($\xi = 1 \dots 4$) is the efficiency at the different optical paths (cf. Fig. 1), and \hat{c}^\dagger [\hat{c}] and \hat{d}^\dagger [\hat{d}] stand for the photon creation [annihilation] operators at the beam splitter output ports. In Eq. (1)

the variables t , $t + \Delta t$ denote the times of detecting heralding events in modes a and b , respectively, while $t + \tau_1$ and $t + \Delta t + \tau_2$ describe the times of detecting events in the detectors placed at the beam splitter output ports c and d , respectively.

In order to evaluate Eq. (1) we utilize the beam splitter transformations and trace over all vacuum modes. Thus, we replace the operators \hat{c} and \hat{d} at the beam splitter outputs with

$$\begin{aligned}\hat{c} &\rightarrow \sqrt{\eta_2(1-T)}\hat{a}_s + \sqrt{\eta_3T}\hat{b}_s \quad \text{and} \\ \hat{d} &\rightarrow \sqrt{\eta_2T}\hat{a}_s - \sqrt{\eta_3(1-T)}\hat{b}_s,\end{aligned}\quad (2)$$

in which T accounts for the used beam splitter transmittance, whereafter we re-write Eq. (1) in terms of the input modes a and b . We model the PDC states as two-mode squeezed vacuum states, shortly *twin beams*. After plugging Eq. (2) in Eq. (1) we arrive at 16 terms, from which only six terms survive. The rest of the terms vanish, when the expectation values are evaluated with the twin beams.

The probability of measuring a four-fold coincidence click is then given by

$$\begin{aligned}P(t, t + \tau_1, t + \Delta t + \tau_2, t + \Delta t) &= \\ &\propto \eta_1\eta_2^2\eta_4T(1-T)\langle\hat{a}_i^\dagger(t)\hat{a}_s^\dagger(t + \tau_1)\hat{a}_s^\dagger(t + \Delta t + \tau_2)\hat{a}_s(t + \Delta t + \tau_2)\hat{a}_s(t + \tau_1)\hat{a}_i(t)\rangle\langle\hat{b}_i^\dagger(t + \Delta t)\hat{b}_i(t + \Delta t)\rangle \\ &+ \eta_1\eta_3^2\eta_4T(1-T)\langle\hat{a}_i^\dagger(t)\hat{a}_i(t)\rangle\langle\hat{b}_i^\dagger(t + \Delta t)\hat{b}_s^\dagger(t + \tau_1)\hat{b}_s^\dagger(t + \Delta t + \tau_2)\hat{b}_s(t + \Delta t + \tau_2)\hat{b}_s(t + \tau_1)\hat{b}_i(t + \Delta t)\rangle \\ &+ \eta_1\eta_2\eta_3\eta_4T^2\langle\hat{a}_i^\dagger(t)\hat{a}_s^\dagger(t + \Delta t + \tau_2)\hat{a}_s(t + \Delta t + \tau_2)\hat{a}_i(t)\rangle\langle\hat{b}_i^\dagger(t + \Delta t)\hat{b}_s^\dagger(t + \tau_1)\hat{b}_s(t + \tau_1)\hat{b}_i(t + \Delta t)\rangle \\ &+ \eta_1\eta_2\eta_3\eta_4(1-T)^2\langle\hat{a}_i^\dagger(t)\hat{a}_s^\dagger(t + \tau_1)\hat{a}_s(t + \tau_1)\hat{a}_i(t)\rangle\langle\hat{b}_i^\dagger(t + \Delta t)\hat{b}_s^\dagger(t + \Delta t + \tau_2)\hat{b}_s(t + \Delta t + \tau_2)\hat{b}_i(t + \Delta t)\rangle \\ &- \eta_1\eta_2\eta_3\eta_4T(1-T)\langle\hat{a}_i^\dagger(t)\hat{a}_s^\dagger(t + \tau_1)\hat{a}_s(t + \Delta t + \tau_2)\hat{a}_i(t)\rangle\langle\hat{b}_i^\dagger(t + \Delta t)\hat{b}_s^\dagger(t + \Delta t + \tau_2)\hat{b}_s(t + \tau_1)\hat{b}_i(t + \Delta t)\rangle \\ &- \eta_1\eta_2\eta_3\eta_4T(1-T)\langle\hat{a}_i^\dagger(t)\hat{a}_s^\dagger(t + \Delta t + \tau_2)\hat{a}_s(t + \tau_1)\hat{a}_i(t)\rangle\langle\hat{b}_i^\dagger(t + \Delta t)\hat{b}_s^\dagger(t + \tau_1)\hat{b}_s(t + \Delta t + \tau_2)\hat{b}_i(t + \Delta t)\rangle,\end{aligned}\quad (3)$$

in which the first two terms describe the effect of the PDC higher photon-number contributions to the coincidences, the two terms in the middle denote the contribution to the coincidences outside the HOM interference dip and the two last terms account for the two-photon quantum interference. We calculate the temporal properties of the HOM interference in terms of the temporal delay Δt and define the visibility of the HOM dip as $\mathcal{V} = \frac{P(\Delta t \rightarrow \infty) - P(\Delta t = 0)}{P(\Delta t \rightarrow \infty)}$. The PDC multiphoton contributions are expected to produce an undesired background to the coincidences and thence, diminish the visibility of the investigated HOM interference dip.

Next, in order to be able to evaluate Eq. (3) we introduce the characteristics of the twin beams. We note that for the sake of simplicity in the following we elaborate the required expectation values for the mode a only. We emphasize that similar considerations apply for the mode b also. The investigated states can be written in the form $|\Psi\rangle = \hat{S}|0\rangle$, in which the narrowband squeezing operator takes the form [31]

$$\hat{S} = \exp\left(\int d\omega S^*(\omega_s)\hat{a}_s(\omega_s)\hat{a}_i(\omega_p - \omega_s) - \int d\omega S(\omega_s)\hat{a}_s^\dagger(\omega_s)\hat{a}_i^\dagger(\omega_p - \omega_s)\right),\quad (4)$$

where ω_s describes the angular frequency of signal and ω_p is that of the pump beam. The joint spectral amplitude of signal and idler is given by $f(\omega_s, \omega_i) = S(\omega_s)\delta(\omega_p - \omega_s - \omega_i)$ with the complex function $S(\omega_s) = r(\omega_s)\exp[i\vartheta(\omega_s)]$ having the amplitude $r(\omega_s)$ and phase $\vartheta(\omega_s)$. The twin beams obey the transformations [31, 32]

$$\begin{aligned}\hat{S}^\dagger\hat{a}_s(\omega_s)\hat{S} &= \hat{a}_s(\omega_s)\beta(\omega_s) - \hat{a}_i^\dagger(\omega_p - \omega_s)\alpha(\omega_s), \\ \hat{S}^\dagger\hat{a}_s^\dagger(\omega_s)\hat{S} &= \hat{a}_s^\dagger(\omega_s)\beta(\omega_s) - \hat{a}_i(\omega_p - \omega_s)\alpha^*(\omega_s)\end{aligned}\quad (5)$$

and

$$\begin{aligned}\hat{S}^\dagger\hat{a}_i(\omega_p - \omega_s)\hat{S} &= \hat{a}_i(\omega_p - \omega_s)\beta(\omega_s) - \hat{a}_s^\dagger(\omega_s)\alpha(\omega_s), \\ \hat{S}^\dagger\hat{a}_i^\dagger(\omega_p - \omega_s)\hat{S} &= \hat{a}_i^\dagger(\omega_p - \omega_s)\beta(\omega_s) - \hat{a}_s(\omega_s)\alpha^*(\omega_s)\end{aligned}\quad (6)$$

for signal and idler, respectively. In Eqs (5) and (6) we utilize the short notations $\beta(\omega_s) = \cosh[r(\omega_s)]$ and $\alpha(\omega_s) = \sinh[r(\omega_s)]\exp[i\vartheta(\omega_s)]$, for which it applies $|\beta(\omega_s)|^2 - |\alpha(\omega_s)|^2 = 1$. We are interested in evaluating Eq. (3) in the

frequency space and take use of the Fourier-transformations

$$\begin{aligned}\hat{a}_\mu(t) &= \frac{1}{\sqrt{2\pi}} \int d\omega \hat{a}_\mu(\omega_\mu) e^{-i\omega_\mu t} \quad \text{and} \\ \hat{a}_\mu^\dagger(t) &= \frac{1}{\sqrt{2\pi}} \int d\omega \hat{a}_\mu^\dagger(\omega_\mu) e^{i\omega_\mu t}\end{aligned}\quad (7)$$

and finally, plug Eqs (5) and (6) together with Eq. (7) in Eq. (3) order to evaluate it.

Following the treatment in Ref. [31] we determine the expectation values required for evaluating Eq. (3). For the detailed derivation see Appendix A. The mean photon flux takes the form

$$\mathcal{N} = \langle \hat{a}_i^\dagger(t) \hat{a}_i(t) \rangle = \langle \hat{a}_s^\dagger(t) \hat{a}_s(t) \rangle = \frac{1}{2\pi} \int d\omega |\alpha(\omega)|^2, \quad (8)$$

and the coherence time of the source can be determined via the normalized first-order coherence $g^{(1)}(\tau) = \frac{\langle \hat{a}_\mu^\dagger(t) \hat{a}_\mu(t+\tau) \rangle}{\langle \hat{a}_\mu^\dagger(t) \hat{a}_\mu(t) \rangle} = \frac{1}{2\pi\mathcal{N}} \int d\omega |\alpha(\omega)|^2 e^{-i\omega\tau}$, which delivers

$$\tau_c = \int d\tau |g^{(1)}(\tau)|^2 = \frac{1}{2\pi\mathcal{N}^2} \int d\omega |\alpha(\omega)|^2 \int d\tilde{\omega} |\alpha(\tilde{\omega})|^2 \underbrace{\frac{1}{2\pi} \int d\tau e^{i(\omega-\tilde{\omega})\tau}}_{=\delta(\omega-\tilde{\omega})} = \frac{1}{2\pi\mathcal{N}^2} \int d\omega |\alpha(\omega)|^4, \quad (9)$$

and which can be measured in an interferometric experiment [33]. Alternatively, the coherence time can also be determined via the second-order correlation of an individual marginal beam that is signal or idler (c.f. Appendix A). Thus, experimentally it can be accessed in a Hanbury-Brown-Twiss experiment of the investigated marginal beam [34, 29]. Luckily, the time-integral over a correlation function is tolerant against the jitter of the detectors and do not disturb the evaluation [33, 35, 36].

Another important figure-of-merit, namely the signal-idler cross-correlation, can be re-written as

$$\langle \hat{a}_i^\dagger(t') \hat{a}_s^\dagger(t) \hat{a}_s(t) \hat{a}_i(t') \rangle = \left[\frac{1}{2\pi} \int d\omega |\alpha(\omega)|^2 \right]^2 + \frac{1}{2\pi} \int d\omega \alpha^*(\omega) \beta(\omega) e^{-i\omega(t'-t)} \frac{1}{2\pi} \int d\tilde{\omega} \alpha(\tilde{\omega}) \beta(\tilde{\omega}) e^{i\tilde{\omega}(t'-t)}, \quad (10)$$

which in the normalized form of

$$g_{s,i}^{(2)}(\tau = t - t') = \frac{\langle \hat{a}_i^\dagger(t') \hat{a}_s^\dagger(t) \hat{a}_s(t) \hat{a}_i(t') \rangle}{\langle \hat{a}_s^\dagger(t) \hat{a}_s(t) \rangle \langle \hat{a}_i^\dagger(t') \hat{a}_i(t') \rangle}, \quad (11)$$

delivers the important information of the coincidences-to-accidentals ratio of the PDC source denoted here with $g_{s,i}^{(2)}(\tau = 0)$. Moreover, Eq. (11) usually can rather conveniently be measured via the coincidence discrimination between signal and idler [37]. Fortunately, the strength of the signal and idler cross-correlation offers means for the quantification of the PDC higher photon-number contributions and can be used as a calibration tool in order to guarantee a high visibility in the HOM interference experiment.

Additionally, we note that the integral over the function $g_{s,i}^{(2)}(\tau) - 1$ delivers a loss-independent estimate of the mean photon flux given as

$$\begin{aligned}\int d\tau [g_{s,i}^{(2)}(\tau) - 1] &= \frac{\int d\tau \frac{1}{2\pi} \int d\omega \alpha^*(\omega) \beta(\omega) e^{i\omega\tau} \frac{1}{2\pi} \int d\tilde{\omega} \alpha(\tilde{\omega}) \beta(\tilde{\omega}) e^{-i\tilde{\omega}\tau}}{\left[\frac{1}{2\pi} \int d\omega |\alpha(\omega)|^2 \right]^2} \\ &= \frac{1}{2\pi\mathcal{N}^2} \int d\omega \alpha^*(\omega) \beta(\omega) \int d\tilde{\omega} \alpha(\tilde{\omega}) \beta(\tilde{\omega}) \underbrace{\frac{1}{2\pi} \int d\tau e^{i(\omega-\tilde{\omega})\tau}}_{=\delta(\omega-\tilde{\omega})} \\ &= \frac{1}{\mathcal{N}^2} \frac{1}{2\pi} \int d\omega |\alpha(\omega)|^2 |\beta(\omega)|^2 = \frac{1}{\mathcal{N}} + \frac{1}{2\pi\mathcal{N}^2} \int d\omega |\alpha(\omega)|^4 = \frac{1}{\mathcal{N}} + \tau_c,\end{aligned}\quad (12)$$

in the last step of which we plugged in the outcome from Eq. (9). The result derived in Eq. (12) is in analog to the case of the broadband multi-mode PDC, in which the time-integrated signal-idler cross-correlation delivers a sum

of two terms, namely the inverse of the mean photon number and the inverse of the number of the excited modes [38]. Moreover, we note that the time integral over the second-order correlation function have recently turned into a practical tool when carrying out quantum optical investigations of other photonic emitters also, such as nanolasers [35].

Further, for the evaluation of Eq. (3) we require a more sophisticated signal-idler cross-correlation term given by

$$\begin{aligned} & \langle \hat{a}_i^\dagger(t) \hat{a}_s^\dagger(t') \hat{a}_s(t'') \hat{a}_i(t) \rangle \\ &= \left(\frac{1}{2\pi} \right)^2 \left[\int d\omega |\alpha(\omega)|^2 \int d\tilde{\omega} |\alpha(\tilde{\omega})|^2 e^{i\tilde{\omega}(t'-t'')} + \int d\omega \alpha^*(\omega) \beta(\omega) e^{-i\omega(t-t')} \int d\tilde{\omega} \alpha(\tilde{\omega}) \beta(\tilde{\omega}) e^{i\tilde{\omega}(t-t'')} \right]. \end{aligned} \quad (13)$$

Finally, in order to estimate the effect of the PDC multiphoton contributions to the coincidences within the HOM interference dip we take use of the expectation value

$$\begin{aligned} & \langle \hat{a}_i^\dagger(t) \hat{a}_s^\dagger(t') \hat{a}_s^\dagger(t'') \hat{a}_s(t') \hat{a}_i(t) \rangle \\ &= \left(\frac{1}{2\pi} \right)^3 \iint d\omega d\tilde{\omega} d\omega' \alpha(\omega) \beta(\omega) |\alpha(\tilde{\omega})|^2 \alpha^*(\omega') \beta(\omega') \left[e^{-i\omega(t''-t)} e^{i\tilde{\omega}(t'-t')} e^{i\omega'(t'-t)} + e^{-i\omega(t'-t)} e^{i\tilde{\omega}(t'-t'')} e^{i\omega'(t''-t)} \right] \\ &+ \left(\frac{1}{2\pi} \right)^3 \iint d\omega d\tilde{\omega} d\omega' \alpha(\omega) \beta(\omega) |\alpha(\tilde{\omega})|^2 \alpha^*(\omega') \beta(\omega') \left[e^{-i\omega(t'-t)} e^{i\tilde{\omega}(t'-t')} e^{i\omega'(t'-t)} + e^{-i\omega(t''-t)} e^{i\tilde{\omega}(t'-t'')} e^{i\omega'(t''-t)} \right] \\ &+ \left(\frac{1}{2\pi} \right)^3 \iint d\omega d\tilde{\omega} d\omega' |\alpha(\omega)|^2 |\alpha(\tilde{\omega})|^2 |\alpha(\omega')|^2 \left[1 + e^{i\tilde{\omega}(t'-t'')} e^{i\omega'(t''-t')} \right]. \end{aligned} \quad (14)$$

3. Simulation of the four-fold coincidences

Next, we perform a simulation of the temporal characteristics of the HOM interference with narrowband PDC sources in the telecommunication wavelength range. Our emphasis lies on understanding the effect of the multiphoton contributions on the HOM dip visibility. For the sake of simplicity we presume that the spectral properties of the two deployed PDC sources are identical. We assume a real-valued Gaussian spectral profile for the marginal beams, thus setting $\vartheta = 0$. We express the spectral amplitude in the form [31]

$$r(\omega_s) = \left(\frac{2\pi\mathcal{F}^2}{\Delta^2} \right)^{1/4} \exp \left(-\frac{[\omega_p/2 - \omega_s]^2}{4\Delta^2} \right), \quad (15)$$

in which Δ is the spectral width of the marginal beams and the degeneracy lies at the angular frequency of $\omega_p/2$. In Eq. (15) the value of \mathcal{F} corresponds to the mean photon flux \mathcal{N} in case the approximation $\sinh[r(\omega)] \approx r(\omega)$ holds.

We plot the marginal spectrum in Fig. 2(a) having the degeneracy wavelength of 1550 nm and a full-width-half-maximum (FWHM) of 0.5 nm. Further, in Fig. 2(b) we illustrate the estimated joint spectral intensity of signal and

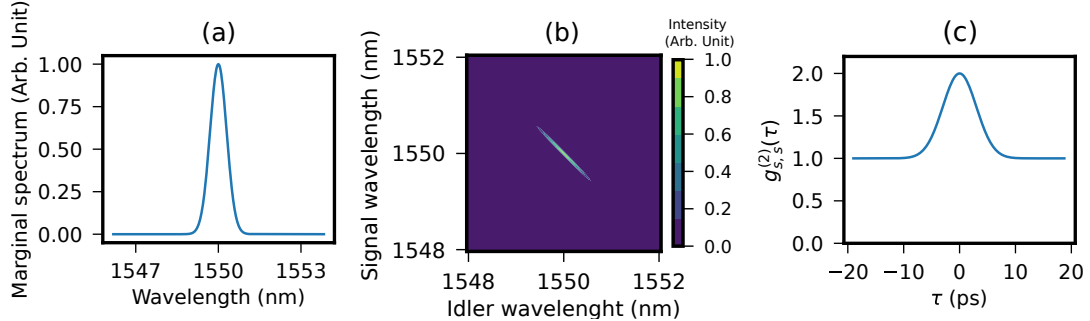


Figure 2: (a) The marginal spectrum of the simulated narrowband PDC source. (b) The corresponding estimated joint spectral intensity of signal and idler. (c) The second-order correlation of an individual marginal beam, here $g_{s,s}^{(2)}(\tau)$.

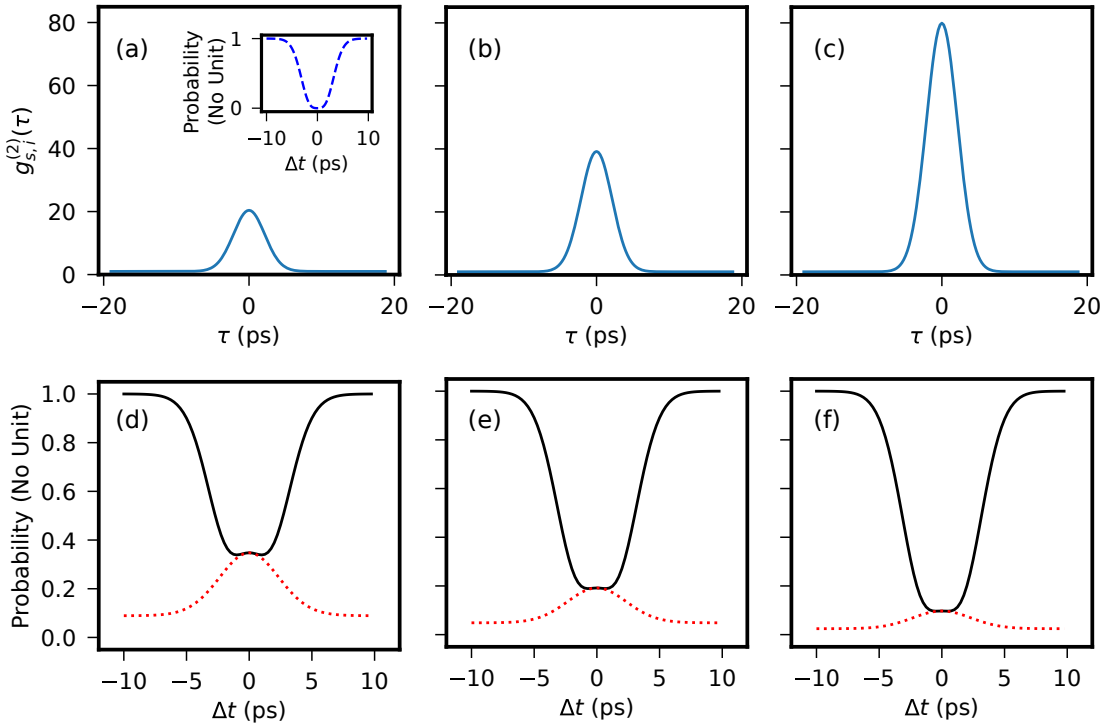


Figure 3: The signal-idler correlation $g_{s,i}^{(2)}(\tau)$ taking the values of approximately (a) 20 (b) 40 and (c) 80 at $\tau = 0$ together with the corresponding temporal characteristics of the HOM interference dips (black lines) resulting in the visibilities close to (d) 0.65 (e) 0.8 and (f) 0.9, respectively. The contribution to the coincidences arriving from the multiphoton effects is plotted in (d-f) with red dotted lines. The inset in (a) illustrates the temporal properties of the HOM interference dip, if the multiphoton effects are neglected.

idler, which as expected is strongly correlated in the frequency space. Moreover, in Fig. 2(c) we evaluate the second-order correlation of an individual marginal beam (here signal) denoted as $g_{s,s}^{(2)}(\tau)$, from which the coherence time of the PDC source can be estimated via the integration that delivers $\tau_c \approx 7.6$ ps (c.f. Appendix A).

We start by investigating the temporal characteristics of the HOM interference in the ideal case of having $T = 1/2$ and $\eta_{\xi=1\dots 4} = 1$. We evaluate the signal-idler cross-correlation at three different photon fluxes that result in $g_{s,i}^{(2)}(\tau = 0)$ -values of approximately 20, 40 and 80 as shown in Figs 3(a-c), respectively. Next, we evaluate the temporal characteristics of the HOM interference dips with Eq. (3) and present them in Figs 3(d-f) that yield the \mathcal{V} -values close to 0.65, 0.8 and 0.9, respectively. Additionally, in Figs 3(d-f) we depict the contribution to the coincidences arriving from the multiphoton effects with red dotted lines. Clearly, their effect cannot be neglected and this background strongly diminishes the visibility of the HOM interference dips. As a consequence, a high value of the signal-idler cross-correlation $g_{s,i}^{(2)}(\tau = 0)$ is required to counteract the effect of multiphoton contributions. To this end, we note that in case the effect of the multiphoton contributions were neglected in Eq. (3), we would expect almost a perfect HOM interference dip as illustrated in the inset in Fig. 3(a).

Next, we investigate the effect of experimental imperfections on the temporal characteristics of the HOM interference and take into account an unbalanced beam splitter ratio and optical losses. Looking at Eq. (3) one can directly conclude that these imperfections contribute differently. The different optical losses in the signal beams' paths influence the scaling of the multiphoton contributions, while the utilization of an unbalanced beam splitter also affects the terms accounting for the HOM interference. We investigate the effect of these imperfections in three different cases. In case (i) we assume that the transmittance of the beam splitter takes the value $T = 0.45$, which is rather typical for integrated optics, while the optical losses in the signal beams' paths are equal. Thereafter, we keep the beam splitter transmittance unchanged at $T = 0.45$ and assume slightly different efficiencies in the paths of the signal beams taking in case (ii) the values $\eta_2 = 2\eta_3 = 0.1$. In case (iii) we regard a stronger imbalance between the optical efficiencies in

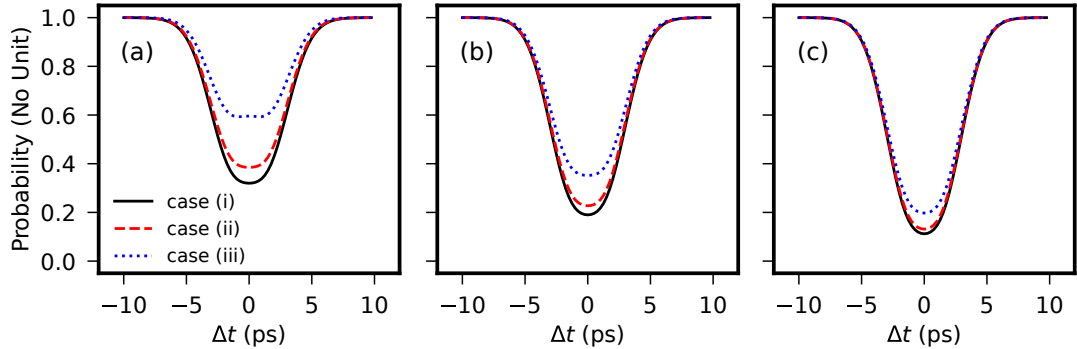


Figure 4: Effect of experimental imperfections on the temporal characteristics of the HOM interference dips. We evaluate Eq. (3) near the values of $g_{s,i}^{(2)}(\tau = 0)$ of (a) 20 (b) 40 and (c) 80 in the three investigated cases (i)-(iii). For the detailed description of the used parameters see the main text.

the signal beams' paths of $\eta_2 = 4\eta_3 = 0.2$. According to our experience values such as considered in cases (ii-iii) are rather typical for experimental arrangements with photon-pair sources in the telecommunication wavelengths [20, 39]. In Fig. 4 we plot for the three investigated cases the temporal properties of the HOM interference at the same values of $g_{s,i}^{(2)}(\tau = 0)$ of about 20, 40 and 80 as in Fig. 3. We note that the utilization of an unbalanced beam splitter in case (i) causes slight changes in the shape of the HOM interference dips and results in the \mathcal{V} -values of approximately 0.68, 0.81 and 0.89, respectively. Due to the unbalanced beam splitter ratio the scaling of the multiphoton effects is slightly lower than in the ideal case presented in Fig. 3, which indeed can even result in a higher visibility. The moderately different losses in the paths of the signal beams in case (ii) diminishes the \mathcal{V} -values further close to 0.61, 0.77 and 0.87, respectively. However, a stronger imbalance in the optical losses of the signal beams' paths such as the one investigated in case (iii) causes a significant drop in the visibilities of the investigated HOM interference dips. In case (iii) the extracted \mathcal{V} -values drop near to 0.41, 0.65 and 0.80, respectively. Evidently, the efficient alignment of the photon-pair setup plays a crucial role in order to achieve a high visibility in the HOM interference experiment.

In order to gain insight, how the multiphoton contributions in the heralded states alter the temporal characteristics of the HOM interference, we illustrate in Fig. 5 the visibility of the HOM interference dip in terms of the value of the signal-idler cross-correlation at $\tau = 0$. When regarding the ideal case (black diamonds) from Fig. 3 that excludes experimental imperfections but takes into account multiphoton contributions we find that the classical limit of $\mathcal{V} = 0.5$, which applies for the coherent states of light, can in our case be rather easily met. For that purpose as low a value as $g_{s,i}^{(2)}(\tau = 0) \gtrsim 13$ is adequate. Interestingly, the HOM interference dip visibility grows fast with increasing signal-idler cross-correlation, but starts to flatten out near $g_{s,i}^{(2)}(\tau = 0) \approx 50$, where $\mathcal{V} \approx 0.84$ can be reached. Beyond that value the visibility of the HOM interference dip grows only modestly. In order to reach the HOM interference dip visibility of $\mathcal{V} \approx 0.9$ the signal-idler cross-correlation needs to be increased to $g_{s,i}^{(2)}(\tau = 0) \approx 80$. In order to suppress the multiphoton contributions, experimentally such high values of signal-idler cross-correlation can be achieved, however, meaning that the pump power has to be low enough, which ultimately leads to lower count rates in the individual marginal beams [39]. For comparison, we illustrate in Fig. 5 the HOM interference dip visibilities also in cases (ii) (red circles) and (iii) (blue triangles). The regarded experimental imperfections do not change the observed behavior of the flattening, only the visibilities reached at the specific values of $g_{s,i}^{(2)}(\tau = 0)$ drop. Especially, if the efficiencies, at which the signal beams are detected, are strongly different such as in case (iii), it becomes difficult to reach a high visibility in the experiment.

4. Conclusions

We investigated the temporal characteristics of the HOM interference between heralded photons from two independent narrowband PDC sources. We derived equations for evaluating the temporal properties of the HOM interference dip, when taking into account the evident multiphoton contributions of PDC and other experimental imperfections

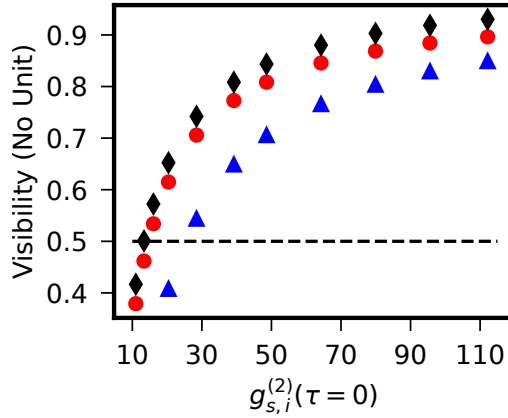


Figure 5: Visibility of the HOM interference dip in terms of the value of $g_{s,i}^{(2)}(\tau = 0)$. When regrading multiphoton contributions but excluding other experimental imperfections (black diamonds) the visibility of the HOM interference dip first grows fast in terms of $g_{s,i}^{(2)}(\tau = 0)$ but then flattens out. When considering experimental imperfections investigated in case (ii) (red circles), a slight deviation towards lower visibilities can be recognized, while the imperfections in case (iii) (blue triangles) already result in a stronger deviation. The dashed horizontal line depicting the classical limit of $\mathcal{V} = 0.5$ provides a guide for the eye.

such as optical losses and an unbalanced beam splitter ratio. We performed a numerical simulation in the telecommunication wavelength range with a narrowband PDC source assuming a Gaussian spectral amplitude. Our numerical simulation shows that the multiphoton contributions rather strongly diminish the visibility of the HOM interference dip. Further, we find out that only modest changes are expected if the transmittance of the beam splitter slightly deviates from that of a perfectly balanced beam splitter as expected for realistic optics components. More crucial is to take care that the optical losses in the signal beams' paths are comparable, since this affects most the scaling of the background from the multiphoton contributions. Strongly different losses on these beam paths results in lower visibilities of the HOM interference dips. Additionally, we showed that the value of the normalized signal-idler cross-correlation $g_{s,i}^{(2)}(\tau = 0)$, which corresponds to the coincidences-to-accidentals ratio, provides a useful tool for selecting a proper photon flux such that high visibility in the HOM interference experiment can be achieved. Most interestingly, the time integral over the function $g_{s,i}^{(2)}(\tau) - 1$ that can usually be extracted in the experiment in a loss-independent manner is proportional to the inverse of the mean photon flux. Altogether, our results show that the PDC multiphoton contributions have to be taken into consideration when investigating HOM interference with heralded PDC sources. We deduce that our results are important for reaching high visibilities in the two-photon quantum interference experiments when utilizing narrowband photon-pair sources.

5. Acknowledgments

We thank Alexander Otterpohl for helpful discussions.

References

- [1] C. K. Hong, Z. Y. Ou, L. Mandel, Measurement of subpicosecond time intervals between two photons by interference, *Phys. Rev. Lett.* 59 (1987) 2044.
- [2] F. Bouchard, A. Sit, Y. Zhang, R. Fickler, F. M. Miatto, Y. Yao, F. Sciarrino, E. Karimi, Two-photon interference: the hong–ou–mandel effect, *Rep. Prog. Phys.* 84 (2021) 012402.
- [3] H. de Riedmatten, I. Marcicic, J. A. W. van Houwelingen, W. Tittel, H. Zbinden, N. Gisin, Long-distance entanglement swapping with photons from separated sources, *Phys. Rev. A* 71 (2005) 050302(R).
- [4] G. Schunk, U. Vogl, F. Sedlmeir, D. V. Strekalov, A. Otterpohl, V. Averchenko, H. G. L. Schwefel, G. Leuchs, C. Marquardt, Frequency tuning of single photons from a whispering-gallery mode resonator to mhz-wide transitions, *J. Mod. Optics* 63 (2016) 2058.
- [5] H. Yu, C. Yuan, R. Zhang, Z. Zhang, H. Li, Y. Wang, G. Deng, L. You, H. Song, Z. Wang, G.-C. Guo, Q. Zhou, Spectrally multiplexed indistinguishable single-photon generation at telecom-band, *Photonics Research* 10 (2022) 1417.

[6] K. Harada, H. Takesue, H. Fukuda, T. Tsuchizawa, T. Watanabe, K. Yamada, Y. Tokura, S. Itabashi, Indistinguishable photon pair generation using two independent silicon wire waveguides, *New J. Phys.* 13 (2011) 065005.

[7] P. Qian, Z. Gu, R. Cao, R. Wen, Z. Y. Ou, J. F. Chen, W. Zhang, Temporal purity and quantum interference of single photons from two independent cold atomic ensembles, *Phys. Rev. Lett.* 117 (2016) 013602.

[8] T. Jeong, Y.-S. Lee, J. Park, H. Kim, H. S. Moon, Quantum interference between autonomous single-photon sources from doppler-broadened atomic ensembles, *Optica* 4 (2017) 1167.

[9] O. Davidson, R. Finkelstein, E. Poem, O. Firstenberg, Bright multiplexed source of indistinguishable single photons with tunable ghz-bandwidth at room temperature, *New J. Phys.* 23 (2021) 073050.

[10] M. Halder, A. Beveratos, N. Gisin, V. Scarani, C. Simon, H. Zbinden, Entangling independent photons by time measurement, *Nature Phys.* 3 (2007) 692.

[11] Y. Xue, A. Yoshizawa, H. Tsuchida, Hong-ou-mandel dip measurements of polarization-entangled photon pairs at 1550 nm, *Optics Express* 18 (2010) 8182.

[12] P. Aboussouan, O. Alibart, D. B. Ostrowsky, P. Baldi, S. Tanzilli, High-visibility two-photon interference at a telecom wavelength using picosecond-regime separated sources, *Phys. Rev. A* 81 (2010) 021801(R).

[13] X. Hua, T. Lunghi, F. Doutre, P. Vergyris, G. Sauder, P. Charlier, L. Labonté, V. D'Auria, A. Martin, S. Tascu, M. P. D. Micheli, S. Tanzilli, O. Alibart, Configurable heralded two-photon fock-states on a chip, *Opt. Express* 29 (2021) 415.

[14] M. Halder, A. Beveratos, R. T. Thew, C. Jorel, H. Zbinden, N. Gisin, High coherence photon pair source for quantum communication, *New J. Phys.* 10 (2008) 023027.

[15] M. Förtsch, J. U. Fürst, C. Wittmann, D. Strekalov, A. Aiello, M. V. Chekhova, C. Silberhorn, G. Leuchs, C. Marquardt, A versatile source of single photons for quantum information processing, *Nature Comm.* 4 (2013) 1818.

[16] R. Mottola, G. Buser, C. Müller, T. Kroh, A. Ahlrichs, S. Ramelow, O. Benson, P. Treutlein, J. Wolters, An efficient, tunable, and robust source of narrow-band photon pairs at the 87rb d1 line, *Opt. Express* 28 (2020) 3159.

[17] V. Sultanov, T. Santiago-Cruz, M. V. Chekhova, Flat-optics generation of broadband photon pairs with tunable polarization entanglement, *Opt. Lett.* 47 (2022) 3872.

[18] O. Cosme, S. Pádua, F. A. Bovino, A. Mazzei, F. Sciarrino, F. D. Martini, Hong-ou-mandel interferometer with one and two photon pairs, *Phys. Rev. A* 77 (2008) 053822.

[19] M. Takeoka, R.-B. Jin, M. Sasaki, Full analysis of multi-photon pair effects in spontaneous parametric down conversion based photonic quantum information processing, *New J. Phys.* 17 (2015) 043030.

[20] T. Günthner, B. Pressl, K. Laiho, J. Geßler, S. Höfling, M. Kamp, C. Schneider, G. Weihs, Broadband indistinguishability from bright parametric downconversion in a semiconductor waveguide, *J. Opt.* 17 (2015) 125201.

[21] I. I. Faruque, G. F. Sinclair, D. Bonneau, T. Ono, C. Silberhorn, M. G. Thompson, J. G. Rarity, Estimating the indistinguishability of heralded single photons using second-order correlation, *Phys. Rev. Applied* 12 (2019) 054029.

[22] K. Laiho, K. N. Cassemiro, C. Silberhorn, Producing high fidelity single photons with optimal brightness via waveguided parametric down-conversion, *Opt. Express* 17 (2009) 22823.

[23] T. Hiemstra, T. Parker, P. Humphreys, J. Tiedau, M. Beck, M. Karpiński, B. Smith, A. Eckstein, W. Kolthammer, I. Walmsley, Pure single photons from scalable frequency multiplexing, *Phys. Rev. Applied* 14 (2020) 014052.

[24] R.-B. Jin, T. Gerrits, M. Fujiwara, R. Wakabayashi, T. Yamashita, S. Miki, H. Terai, R. Shimizu, M. Takeoka, M. Sasaki, Spectrally resolved hong-ou-mandel interference between independent photon sources, *Optics Express* 23 (2015) 28836.

[25] K. Laiho, B. Pressl, A. Schlager, H. Suchomel, M. Kamp, S. Höfling, C. Schneider, G. Weihs, Uncovering dispersion properties in semiconductor waveguides to study photon-pair generation, *Nanotechnology* 27 (2016) 434003.

[26] T. S. Iskhakov, K. Y. Spasibko, M. V. Chekhova, G. Leuchs, Macroscopic hong-ou-mandel interference, *New J. Phys.* 15 (2013) 093036.

[27] P. M. Alsing, R. J. Birrittella, C. C. Gerry, J. Mimih, P. L. Knights, Extending the hong-ou-mandel effect: The power of nonclassicality, *Phys. Rev. A* 105 (2022) 013712.

[28] K. H. Luo, H. Herrmann, S. Krapick, B. Brecht, R. Ricken, V. Quiring, H. Suche, W. Sohler, C. Silberhorns, Direct generation of genuine single-longitudinal-mode narrowband photon pairs, *New J. Phys.* 17 (2015) 073039.

[29] G. Shafee, D. V. Strekalov, A. Otterpohl, F. Sedlmeir, G. Schunk, U. Vogl, H. G. L. Schwefel, G. Leuchs, C. Marquardt, Nonlinear power dependence of the spectral properties of an optical parametric oscillator below threshold in the quantum regime, *New J. Phys.* 22 (2020) 073045.

[30] V. Averchenko, D. Sych, C. Marquardt, G. Leuchs, Efficient generation of temporally shaped photons using nonlocal spectral filtering, *Phys. Rev. A* 101 (2020) 013808.

[31] R. Loudon, *The quantum theory of light*, 3rd Edition, Oxford university Press, 2000.

[32] S. M. Barnett, P. M. Rendmore, *Methods in theoretical quantum optics*, Oxford University Press, 1997.

[33] B. Blauensteiner, I. Herbaus, S. Betelli, A. Poppe, H. Hübel, Photon bunching in parametric down-conversion with continuous-wave excitation, *Phys. Rev. A* 79 (2009) 063846.

[34] R. H. Brown, R. Q. Twiss, A test of a new type of stellar interferometer on sirius, *Nature* 178 (1956) 1046.

[35] S. Kreinberg, W. W. Chow, J. W. C. Schneider, C. Gies, F. Jahnke, S. Höfling, M. Kamp, S. Reitzenstein, Emission from quantum-dot high- β microcavities: transition from spontaneous emission to lasing and the effects of superradiant emitter coupling, *Light: Science & Applications* 6 (2017) 17030.

[36] K. Laiho, T. Dirmeier, M. Schmidt, S. Reitzenstein, C. Marquardt, Measuring higher-order photon correlations of faint quantum light: a short review, *Phys. Lett. A* 435 (2022) 128059.

[37] M. Förtsch, G. Schunk, J. U. Fürst, D. Strekalov, T. Gerrits, M. J. Stevens, F. Sedlmeir, H. G. L. Schwefel, S. W. Nam, G. Leuchs, C. Marquardt, Highly efficient generation of single-mode photon pairs from a crystalline whispering-gallery-mode resonator source, *Phys. Rev. A* 91 (2015) 023812.

[38] A. Christ, K. Laiho, A. Eckstein, K. N. Cassemiro, C. Silberhorn, Probing multimode squeezing with correlation functions, *New. J. Phys.* 13 (2011) 033027.

[39] H. Chen, S. Auchter, M. Prilmüller, A. Schlager, T. Kauten, K. Laiho, B. Pressl, H. Suchomel, M. Kamp, S. Höfling, C. Schneider, G. Weihs, Invited article: Time-bin entangled photon pairs from bragg-reflection waveguides, *APL Photonics* 3 (2018) 080804.

Appendix A. Derivation of the expectation values

In this appendix we derive for the completeness the expectation values required for evaluating Eq. (3). We follow the treatment in Ref. [31], employ the Fourier-transforms in Eq. (7) to replace the time domain with the frequency space and utilize the transformations in Eqs (5) and (6). We start by evaluating

$$\begin{aligned} \langle \hat{a}_s^\dagger(t) \hat{a}_s(t+\tau) \rangle &= \frac{1}{2\pi} \iint d\omega d\tilde{\omega} e^{i\omega t} e^{-i\tilde{\omega}(t+\tau)} \langle 0 | \hat{S}^\dagger \hat{a}_s^\dagger(\omega) \hat{a}_s(\tilde{\omega}) \hat{S} | 0 \rangle \\ &= \frac{1}{2\pi} \iint d\omega d\tilde{\omega} e^{i\omega t} e^{-i\tilde{\omega}(t+\tau)} \alpha^*(\omega) \alpha(\tilde{\omega}) \underbrace{\langle \hat{a}_i(\omega_p - \omega) \hat{a}_i^\dagger(\omega_p - \tilde{\omega}) \rangle}_{=\delta(\omega - \tilde{\omega})} \\ &= \frac{1}{2\pi} \iint d\omega |\alpha(\omega)|^2 e^{-i\omega\tau}, \end{aligned} \quad (\text{A.1})$$

in which we used the relation $\hat{S} \hat{S}^\dagger = 1$ and the commutator $[\hat{a}_\mu^\dagger(\omega), \hat{a}_\mu(\tilde{\omega})] = \delta(\omega - \tilde{\omega})$. Next, we investigate the second-order correlation of an individual marginal beam (here signal) that takes the form

$$\begin{aligned} \langle \hat{a}_s^\dagger(t) \hat{a}_s^\dagger(t') \hat{a}_s(t') \hat{a}_s(t) \rangle &= \left(\frac{1}{2\pi} \right)^2 \iint d\omega_1 d\omega_2 d\omega_3 d\omega_4 e^{i\omega_1 t} e^{i\omega_2 t'} e^{-i\omega_3 t'} e^{-i\omega_4 t} \langle 0 | \hat{S}^\dagger \hat{a}_s^\dagger(\omega_1) \hat{a}_s^\dagger(\omega_2) \hat{a}_s(\omega_3) \hat{a}_s(\omega_4) \hat{S} | 0 \rangle \\ &= \left(\frac{1}{2\pi} \right)^2 \iint d\omega_1 d\omega_2 d\omega_3 d\omega_4 e^{i\omega_1 t} e^{i\omega_2 t'} e^{-i\omega_3 t'} e^{-i\omega_4 t} \underbrace{\langle \hat{a}_i^\dagger(\omega_p - \omega_1) \hat{a}_i^\dagger(\omega_p - \omega_2) \hat{a}_i(\omega_p - \omega_3) \hat{a}_i(\omega_p - \omega_4) \rangle}_{=\delta(\omega_2 - \omega_3)\delta(\omega_1 - \omega_4) + \delta(\omega_1 - \omega_3)\delta(\omega_2 - \omega_4)} \alpha^*(\omega_1) \alpha^*(\omega_2) \alpha(\omega_3) \alpha(\omega_4) \end{aligned} \quad (\text{A.2})$$

which we re-write as

$$\langle \hat{a}_s^\dagger(t) \hat{a}_s^\dagger(t') \hat{a}_s(t') \hat{a}_s(t) \rangle = \left(\frac{1}{2\pi} \right)^2 \left[\int d\omega |\alpha(\omega)|^2 \right]^2 + \frac{1}{2\pi} \int d\omega |\alpha(\omega)|^2 e^{i\omega(t-t')} \frac{1}{2\pi} \int d\tilde{\omega} |\alpha(\tilde{\omega})|^2 e^{-i\tilde{\omega}(t-t')}. \quad (\text{A.3})$$

Thence, the normalized form of the second-order correlation of an individual marginal beam delivers

$$\begin{aligned} g_{s,s}^{(2)}(\tau = t - t') &= \frac{\langle \hat{a}_s^\dagger(t) \hat{a}_s^\dagger(t') \hat{a}_s(t') \hat{a}_s(t) \rangle}{\langle \hat{a}_s^\dagger(t) \hat{a}_s(t) \rangle \langle \hat{a}_s^\dagger(t') \hat{a}_s(t') \rangle} \\ &= 1 + \frac{1}{2\pi N} \int d\omega |\alpha(\omega)|^2 e^{i\omega\tau} \frac{1}{2\pi N} \int d\tilde{\omega} |\alpha(\tilde{\omega})|^2 e^{-i\tilde{\omega}\tau}, \end{aligned} \quad (\text{A.4})$$

which can also be used for evaluating the coherence time via $\tau_c = \int d\tau (g_{s,s}^{(2)}(\tau) - 1)$.

Further, we determine the cross-correlation term

$$\begin{aligned} \langle \hat{a}_i^\dagger(t) \hat{a}_s^\dagger(t') \hat{a}_s(t'') \hat{a}_i(t) \rangle &= \left(\frac{1}{2\pi} \right)^2 \iint d\omega_1 d\omega_2 d\omega_3 d\omega_4 e^{i\omega_1 t} e^{i\omega_2 t'} e^{-i\omega_3 t''} e^{-i\omega_4 t} \langle 0 | \hat{S}^\dagger \hat{a}_i^\dagger(\omega_1) \hat{a}_s^\dagger(\omega_2) \hat{a}_s(\omega_3) \hat{a}_i(\omega_4) \hat{S} | 0 \rangle \end{aligned} \quad (\text{A.5})$$

which requires the expectation value

$$\begin{aligned}
& \langle \hat{a}_i^\dagger(\omega_1) \hat{a}_s^\dagger(\omega_2) \hat{a}_s(\omega_3) \hat{a}_i(\omega_4) \rangle \\
&= \langle \hat{a}_s(\omega_p - \omega_1) \alpha^*(\omega_p - \omega_1) [\hat{a}_s^\dagger(\omega_2) \beta(\omega_2) - \hat{a}_i(\omega_p - \omega_2) \alpha^*(\omega_2)] \\
&\quad \otimes [\hat{a}_s(\omega_3) \beta(\omega_3) - \hat{a}_i^\dagger(\omega_p - \omega_3) \alpha^*(\omega_3)] \hat{a}_s^\dagger(\omega_p - \omega_4) \alpha(\omega_p - \omega_4) \rangle \\
&= \alpha^*(\omega_p - \omega_1) \alpha(\omega_p - \omega_4) \beta(\omega_2) \beta(\omega_3) \underbrace{\langle \hat{a}_s(\omega_p - \omega_1) \hat{a}_s^\dagger(\omega_2) \hat{a}_s(\omega_3) \hat{a}_s^\dagger(\omega_p - \omega_4) \rangle}_{=\delta((\omega_p - \omega_1 - \omega_2) \delta((\omega_p - \omega_4 - \omega_3))} \\
&\quad + \alpha^*(\omega_p - \omega_1) \alpha(\omega_p - \omega_4) \alpha^*(\omega_2) \alpha(\omega_3) \underbrace{\langle \hat{a}_s(\omega_p - \omega_1) \hat{a}_i^\dagger(\omega_p - \omega_2) \hat{a}_i(\omega_p - \omega_3) \hat{a}_s^\dagger(\omega_p - \omega_4) \rangle}_{=\delta(\omega_1 - \omega_4) \delta(\omega_2 - \omega_3)}.
\end{aligned} \tag{A.6}$$

Eventually, Eq. (A.5) takes the form

$$\begin{aligned}
\langle \hat{a}_i^\dagger(t) \hat{a}_s^\dagger(t') \hat{a}_s(t'') \hat{a}_i(t) \rangle &= \frac{1}{2\pi} \int d\omega \alpha^*(\omega) \beta(\omega) e^{-i\omega(t-t')} \frac{1}{2\pi} \int d\tilde{\omega} \alpha(\tilde{\omega}) \beta(\tilde{\omega}) e^{i\omega(t-t'')} \\
&+ \frac{1}{2\pi} \int d\omega |\alpha(\omega_p - \omega)|^2 \frac{1}{2\pi} \int d\tilde{\omega} |\alpha(\tilde{\omega})|^2 e^{i\tilde{\omega}(t'-t'')},
\end{aligned} \tag{A.7}$$

which further reduces to Eq. (10) if $t' = t''$.

Finally, we evaluate the effect of the multiphoton contributions to the coincidences, which can be extracted via

$$\begin{aligned}
& \langle \hat{a}_i^\dagger(t) \hat{a}_s^\dagger(t') \hat{a}_s^\dagger(t'') \hat{a}_s(t'') \hat{a}_s(t') \hat{a}_i(t) \rangle \\
&= \left(\frac{1}{2\pi} \right)^3 \iint d\omega_1 d\omega_2 d\omega_3 d\omega_4 d\omega_5 d\omega_6 e^{i\omega_1 t} e^{i\omega_2 t'} e^{i\omega_3 t''} e^{-i\omega_4 t''} e^{-i\omega_5 t'} e^{-i\omega_6 t} \langle 0 | \hat{S}^\dagger \hat{a}_i^\dagger(\omega_1) \hat{a}_s^\dagger(\omega_2) \hat{a}_s^\dagger(\omega_3) \hat{a}_s(\omega_4) \hat{a}_s(\omega_5) \hat{a}_i(\omega_6) \hat{S} | 0 \rangle.
\end{aligned} \tag{A.8}$$

In order to evaluate Eq. (A.8) we determine the expectation value

$$\begin{aligned}
& \langle \hat{a}_i^\dagger(\omega_1) \hat{a}_s^\dagger(\omega_2) \hat{a}_s^\dagger(\omega_3) \hat{a}_s(\omega_4) \hat{a}_s(\omega_5) \hat{a}_i(\omega_6) \rangle = \langle \hat{a}_s(\omega_p - \omega_1) \alpha^*(\omega_p - \omega_1) [\hat{a}_s^\dagger(\omega_2) \beta(\omega_2) - \hat{a}_i(\omega_p - \omega_2) \alpha^*(\omega_2)] \\
&\quad \otimes [\hat{a}_s^\dagger(\omega_3) \beta(\omega_3) - \hat{a}_i(\omega_p - \omega_3) \alpha^*(\omega_3)] [\hat{a}_s(\omega_4) \beta(\omega_4) - \hat{a}_i^\dagger(\omega_p - \omega_4) \alpha(\omega_4)] \\
&\quad \otimes [\hat{a}_s(\omega_5) \beta(\omega_5) - \hat{a}_i^\dagger(\omega_p - \omega_5) \alpha(\omega_5)] \hat{a}_s^\dagger(\omega_p - \omega_6) \alpha(\omega_p - \omega_6) \rangle \\
&= \alpha^*(\omega_p - \omega_1) \beta(\omega_2) \alpha^*(\omega_3) \beta(\omega_4) \alpha(\omega_5) \alpha(\omega_p - \omega_6) \underbrace{\langle \hat{a}_s(\omega_p - \omega_1) \hat{a}_s^\dagger(\omega_2) \hat{a}_i(\omega_p - \omega_3) \hat{a}_s(\omega_4) \hat{a}_i^\dagger(\omega_p - \omega_5) \hat{a}_s^\dagger(\omega_p - \omega_6) \rangle}_{=\delta(\omega_p - \omega_6 - \omega_4) \delta(\omega_3 - \omega_5) \delta(\omega_p - \omega_1 - \omega_2)} \\
&\quad + \alpha^*(\omega_p - \omega_1) \beta(\omega_2) \alpha^*(\omega_3) \alpha(\omega_4) \beta(\omega_5) \alpha(\omega_p - \omega_6) \underbrace{\langle \hat{a}_s(\omega_p - \omega_1) \hat{a}_s^\dagger(\omega_2) \hat{a}_i(\omega_p - \omega_3) \hat{a}_i^\dagger(\omega_p - \omega_4) \hat{a}_s(\omega_5) \hat{a}_s^\dagger(\omega_p - \omega_6) \rangle}_{=\delta(\omega_p - \omega_6 - \omega_5) \delta(\omega_3 - \omega_4) \delta(\omega_p - \omega_1 - \omega_2)} \\
&\quad + \alpha^*(\omega_p - \omega_1) \alpha^*(\omega_2) \beta(\omega_3) \beta(\omega_4) \alpha(\omega_5) \alpha(\omega_p - \omega_6) \underbrace{\langle \hat{a}_s(\omega_p - \omega_1) \hat{a}_i(\omega_p - \omega_2) \hat{a}_s^\dagger(\omega_3) \hat{a}_s(\omega_4) \hat{a}_i^\dagger(\omega_p - \omega_5) \hat{a}_s^\dagger(\omega_p - \omega_6) \rangle}_{=\delta(\omega_p - \omega_6 - \omega_4) \delta(\omega_2 - \omega_5) \delta(\omega_p - \omega_1 - \omega_3)} \\
&\quad + \alpha^*(\omega_p - \omega_1) \alpha^*(\omega_2) \beta(\omega_3) \alpha(\omega_4) \beta(\omega_5) \alpha(\omega_p - \omega_6) \underbrace{\langle \hat{a}_s(\omega_p - \omega_1) \hat{a}_i(\omega_p - \omega_2) \hat{a}_s^\dagger(\omega_3) \hat{a}_i^\dagger(\omega_p - \omega_4) \hat{a}_s(\omega_5) \hat{a}_s^\dagger(\omega_p - \omega_6) \rangle}_{=\delta(\omega_p - \omega_6 - \omega_5) \delta(\omega_2 - \omega_4) \delta(\omega_p - \omega_1 - \omega_3)} \\
&\quad + \alpha^*(\omega_p - \omega_1) \alpha^*(\omega_2) \alpha^*(\omega_3) \alpha(\omega_4) \alpha(\omega_5) \alpha(\omega_p - \omega_6) \\
&\quad \cdot \underbrace{\langle \hat{a}_s(\omega_p - \omega_1) \hat{a}_i(\omega_p - \omega_2) \hat{a}_i(\omega_p - \omega_3) \hat{a}_i^\dagger(\omega_p - \omega_4) \hat{a}_i^\dagger(\omega_p - \omega_5) \hat{a}_s^\dagger(\omega_p - \omega_6) \rangle}_{=\delta(\omega_6 - \omega_1) [\delta(\omega_3 - \omega_4) \delta(\omega_2 - \omega_5) + \delta(\omega_2 - \omega_4) \delta(\omega_3 - \omega_5)]},
\end{aligned} \tag{A.9}$$

in the final form of which only few terms survive. Plugging Eq. (A.9) in Eq. (A.8) results in Eq. (14).